Package Integrated Vapor Chamber Heat Spreaders

Cameron Nelson
Amkor Technology
Tempe, AZ, USA
Cameron.Nelson@Amkor.com

SangHyuk Kim
Amkor Technology
Incheon, Republic of Korea
SangHyuk.Kim@Amkor.co.kr

***Abstract*— In Flip Chip Ball Grid Array (FCBGA) packages that require the protection and mechanical benefits of an integrated heat spreader, a package integrated vapor chamber heat spreader can offer significant thermal enhancement compared to a pure copper heat spreader. This study investigates the unique characteristics and challenges of integrating a vapor chamber heat spreader onto a FCBGA package and proposes a methodology to quantify the effective thermal conductivity of the vapor chamber under different conditions using finite element analysis. Test results indicate that the effective thermal conductivity of the vapor chamber varies depending on the system cooling solution's thermal resistance, and for most cases, offers significant thermal enhancement over a pure copper heat spreader. An FCBGA thermal test vehicle was constructed to evaluate the vapor chamber heat spreaders. With a high resistance cooling solution comprised of an aluminum heat sink and pad type TIM II, the package integrated vapor chamber heat spreader offered a 12.5°C reduction in junction temperature at 120 W power compared to a standard copper heat spreader. With a low resistance cooling solution, a copper heat sink and grease type TIM II, the package integrated vapor chamber heat spreader offered a 4.2°C reduction in junction temperature compared to a standard copper heat spreader. Using a finite element analysis (FEA) method to extract the effective thermal conductivity of the vapor chamber heat spreaders, it was found that under the aluminum heat sink and pad type TIM II test condition, the vapor chamber achieved an effective thermal conductivity of 11,750 W/m*K. Under the copper heat sink and grease type TIM II test, the vapor chamber heat spreader was found to achieve an effective thermal conductivity of 3,495 W/m*K.**

Keywords—FCBGA, vapor chamber, heat spreader, packaging, thermal enhancement.

I. Introduction

With continuous increases in computational demand in nearly all semiconductor market segments, even historically lower power packaging is being driven into challenging thermal management situations. Node shrink alone is reaching a limit in maintaining track with Moore's law. The economics and yield challenges of large monolithic system on chip (SoC) designs are driving the development of silicon disaggregation or chiplet adoption. This and trends in total power dissipation are driving the development of extremely low thermal resistance cooling systems. High-performance systems may implement a combination of heat pipes, vapor chambers, or liquid cooling, driving sink-to-ambient thermal resistance less than 0.5°C/W [1]. These low resistance cooling solutions translate to the package now comprising a much larger percentage of the total junction-to-ambient thermal resistance. As a result, these trends are forcing the need for thermal enhancement closer to the silicon than ever before.

II. Vapor Chamber

A vapor chamber (VC) is a type of two-phase passive heat transfer device that can achieve an effective thermal conductivity more than 20 times greater than that of copper (Cu), which already has one of the highest material thermal conductivities. A vapor chamber has the same working principal as a heat pipe, but simply in a planar form factor. A typical vapor chamber consists of a copper enclosure containing a vacuum-sealed internal cavity, Fig. 1. Within this cavity there is a copper wick structure and small amount of working fluid (commonly water). The mechanism behind the heat transfer takes advantage of water's high heat of vaporization. Near the heat source (the object being cooled), energy converts the working fluid to vapor. The hot vapor then spreads to the cooler outer areas away from the heat source where it releases its latent heat as it condenses back into water. Finally, the wick structure draws the water back to the heat source through capillary action [2]. A critical factor driving the effective thermal conductivity a vapor chamber is the ratio of heat source area to total vapor chamber size. Typically, the greater the size of the vapor chamber relative to the heat source, the higher the efficiency and therefore thermal conductivity that can be achieved.

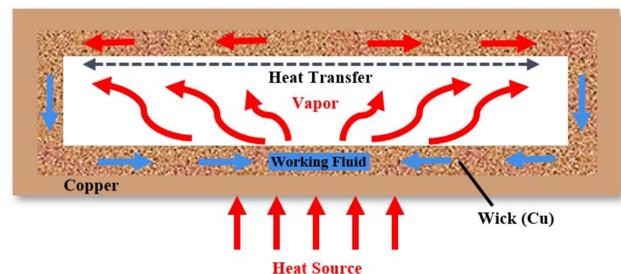

Fig. 1. Vapor chamber construction and function.

III. Package Heat Spreaders

Package heat spreaders can offer a variety of benefits such as protection of the silicon, warpage management, increased reliability, and thermal enhancement, however, there are tradeoffs for every situation.

A. Thermal Enhancement

For system cooling solutions with extremely low thermal resistances, such as a high-performance graphics processing unit (GPU), it may be beneficial to omit a heat spreader and

2377-5726/23/$31.00 ©2023 IEEE
DOI 10.1109/ECTC51909.2023.00271

its associated additional layer of thermal interface material in favor of directly contacting the system cooling solution. In this type of configuration, the system cooling solution likely implements vapor chamber or heat pipe embedded heat sinks with highly forced convection or liquid cooling. Alternatively, in applications with higher thermal resistance cooling solutions, a copper heat spreader and low resistance TIM I can spread heat over a larger area, improving the efficiency, effectively the thermal resistance, of the external cooling solution.

B. *Robustness and Reliability*

Applying a thermal interface material and mounting an external heat sink to an exposed silicon package can be challenging to maintain quality control and avoid the risk of silicon damage by chipping. In addition, thermal interface materials in an exposed silicon package are typically much more prone to degradation due to pump out and dry out. When a package implements an integrated heat spreader it protects the silicon during heat sink assembly and offers a greater surface area for TIM II application and managing heat sink tilt. Lidded packages are typically associated with having better longevity and reliability compared to an exposed silicon package for these reasons.

IV. Vapor Chamber Heat Spreader

For many years, vapor chambers have been widely implemented in system cooling solutions for high power computing application spaces from graphics cards to data centers. With advances in manufacturing technology, more recently ultra-thin vapor chamber heat spreaders are being implemented into non-traditional applications such as premium smartphones [3]. Despite this, there has yet to be a mainstream adoption of integrating the vapor chamber into advanced flip chip packages.

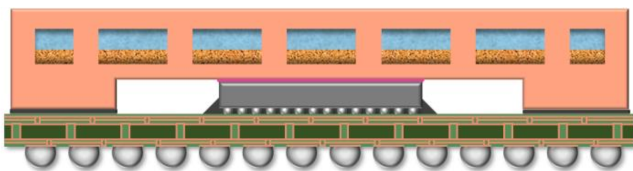

Fig. 2. Package integrated vapor chamber heat spreader.

A. *Package Size*

A critical design metric of a vapor chamber is the ratio of heat source area to the total area of the vapor chamber. Packages are clearly intentionally designed to have as small of a footprint as possible, so the available area for a vapor chamber is severely limited. Considering this, a package integrated vapor chamber, Fig. 2, is only effective if the heat source (silicon chip or hot spots within the chip design) is small relative to the total package area, which may be much larger to accommodate a high number of I/O signals. Chip designs with highly concentrated heat fluxes can benefit even further from the high thermal conductivity of vapor chamber.

B. *Cost Reduction of Vapor Chamber Manufacturing*

Historically, high-power FCBGA packages would typically already implement advanced system cooling solutions, so the addition of a package-level vapor chamber would offer little benefit. However, with thermal management becoming more demanding in many more application spaces and the cost and scalability of vapor chamber manufacturing improving, opportunities have opened significantly for a wider range of applications. Now, vapor chambers and other advanced thermal solutions are economically viable across mid- to upper-range markets. Considering a cost sensitive application, if thermal enhancement it required, it may be more cost effective to implement a package vapor chamber heat spreader rather than upgrade the entire system cooling solution or heat sink to accommodate an increase in package power dissipation.

C. *High Temperature Internal Pressure*

A BGA style package will go through at least two reflow cycles: first to attach the BGA to the package substrate and second to attach the package to the system board. Additional reflow cycles could be considered for any preconditioning or rework. A typical SAC reflow profile may see temperatures up to 260°C for a brief period. Using saturated steam tables from literature, the internal pressure of a vapor chamber can be estimated. At peak reflow temperature, the internal pressure can reach more than 4 MPa, Fig. 3.

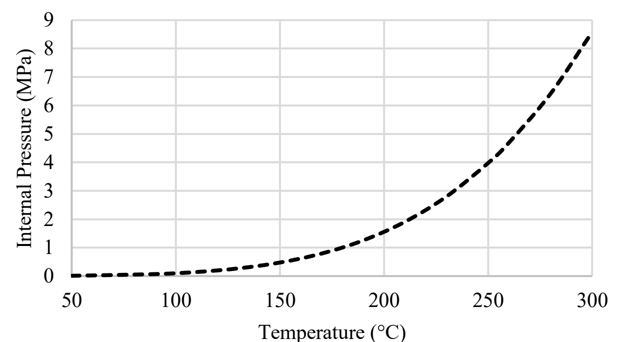

Fig. 3. Internal pressure of a vapor chamber versus temperature.

With the latest manufacturing technology, vapor chambers can be constructed extremely thin. While a thin vapor chamber is ideal in terms of packaging integration, the vapor chamber needs to have enough structural integrity to withstand the extreme pressures induced during a BGA reflow cycle. A few design characteristics seen in Fig. 4 allow this to be accomplished: 1.) Having a wall thickness > 0.8 mm of copper and 2.) Designing copper structural columns into the cavity connecting the top and bottom walls to provide compressive and tensile (during high temperature) rigidity.

To evaluate the impact of this high pressurization on the TIM I and package warpage, a simulation study was conducted. High deformation of a VC heat spreader on an FCBGA package could degrade the thermal interface

material or cause unexpected warpage behavior. The modeling was conclusive that with adequate VC wall thickness (> 1.0 mm) and copper support columns, the deformation and warpage influence was insignificant at peak internal pressures during BGA reflow.

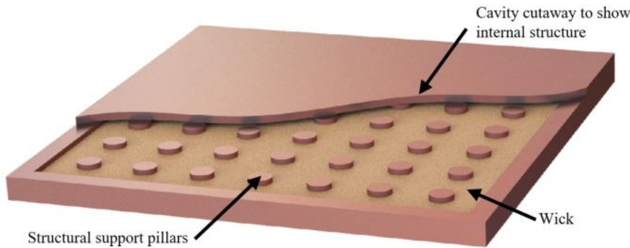

Fig. 4. Vapor chamber heat spreader cutaway showing internal construction.

D. Package Assembly Considerations

In high thermal performance FCBGA packages, a gel type thermal interface material is commonly preferred. Gel TIMs are typically loaded with alumina or silver filler particles and undergo a crosslinking cure at high temperature [4]. Once cured, they still exhibit relatively strong cohesive and adhesive strengths, but can offer high elongation and maintain low interfacial contact resistance [5]. The characteristics make them ideal for FCBGAs with large die. A gel type TIM is also a favored selection for a package integrated vapor chamber heat spreader because of the possibility of expansion during BGA reflow or package surface mount technology (SMT) assembly. A key assembly quality monitor for TIM I materials is inspection by scanning acoustic tomography, SAT, which offers a non-destructive view of the TIM quality beneath the heat spreader. SAT inspection can capture voids or defects within the package by detecting the acoustic impedance of varying material densities. However, SAT can not image through the internal cavity vacuum of a vapor chamber. Therefore, TIM inspection by SAT is not a viable approach for a package integrated vapor chamber heat spreader.

To understand the potential thermal performance enhancement of a vapor chamber integrated at the package level rather than the system level, it is critical to evaluate the package geometry (body size versus die size), system cooling solution (heat sink base material, size, and effective heat transfer), and overall system cost.

V. Thermal Test Setup

In this study, thermal test vehicle packages were constructed to characterize the thermal impact of the vapor chamber heat spreaders. The packages consisted of a 60 mm x 60 mm FCBGA with a 12-layer cored substrate. A thermal test chip was used to accurately control power dissipation and preform silicon temperature measurements. The thermal chip is diced from a wafer containing an array of unit cells with each individual cell containing a resistive heater and resistive temperature device (RTD). The test chip was 25 mm x 25 mm in size, with a thickness of 0.780 mm. The RTDs designed into the thermal test chip allow for localized silicon temperature measurement through four-point sensing. The packages were mounted to a test board, which routed the power delivery and signal outputs to a data acquisition system. The data acquisition systems controls the power supplied to the individual unit cell heaters on the test chip as well as records the four-point voltage measurement from the RTD. For this study, equivalent power was supplied to each unit cell in the test chip to provide uniform heating across the total chip area. The total power applied was 120W for all test legs to achieve a baseline target junction temperature of about 60°C with an aluminum (Al) heat sink and grease TIM II. A heat sink is mounted to the package and test board (Fig. 5) to provide cooling. The heat sink selection for the design of experiments (DOE) is described in the next section.

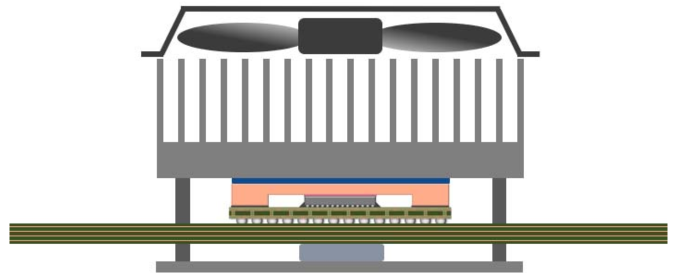

Fig. 5. Test setup schematic.

To capture the range of thermal performance of the vapor chamber heat spreaders, a design of experiments was outlined to encompass a spectrum of possible application conditions, (Table 1). The effective conductivity of a vapor chamber is expected to be dependent on the external heat transfer conditions, which in this case, translates to the TIM II and external cooling solution. TIM II selection will influence the amount of heat spreading within the package. A high TIM II thermal resistance will force greater heat spreading within the package, whereas a low resistance material will allow for a more direct heat flow path with less spreading in the package. Further along the heat conduction path is the heat sink base. The base material thermal conductivity determines the heat spreading resistance. Comparing two common heat sink materials, aluminum and copper, aluminum, with its lower thermal conductivity has a higher spreading resistance than a heat sink constructed of copper. This means it is more advantageous to spread heat over a larger area before contacting an aluminum heat sink. The aluminum heat sink is expected to show a greater difference between a vapor chamber heat spreader and a pure copper heat spreader.

Two heat sinks were selected, aluminum and copper, both with equivalent dimensions: 90 x 120 mm in size with a 7-mm base thickness. Fans were attached to the heat sinks and speed was constant for all legs. Two TIM II materials were selected. For a high thermal resistance condition, a pad type material was selected which had an effective thermal resistance of 80 °C/W*mm^2. For a low resistance condition, a grease type TIM II was selected which achieves about 15 °C/W*mm^2 thermal resistance.

TABLE I. THERMAL TEST DOE

Leg	Heat Spreader	TIM II	Heat Sink
1	1.5T Cu SPL	Pad Type 80 °C/W*mm^2	Aluminum
2	Vapor Chamber	Pad Type 80 °C/W*mm^2	Aluminum
3	1.5T Cu SPL	Grease 15 °C/W*mm^2	Aluminum
4	Vapor Chamber	Grease 15 °C/W*mm^2	Aluminum
5	1.5T Cu SPL	Grease 15 °C/W*mm^2	Copper
6	Vapor Chamber	Grease 15 °C/W*mm^2	Copper

Non-critical variables in this test were fixed between all legs: heat sink clamping pressure, fan speed and ambient temperature. Accurate absolute values for TIM II resistance are not required for this study because all measurements will be a relative comparison between heat spreader types and the test conditions will be consistent. Between comparison pairs in the DOE (legs 1&2, 3&4 and 5&6), the only variable changed is the heat spreader type.

VI. THERMAL MEASUREMENTS

One of the most common metrics to characterize thermal performance of high power FCBGA packages is the junction-to-case thermal resistance, referred to as θ_{JC} (1). In an FCBGA package, θ_{JC} defines the thermal resistance of a package along the path of silicon, thermal interface material (TIM I) and heat spreader.

$$\theta_{JC} = \frac{T_{junction} - T_{case}}{Power} \quad (1)$$

The purpose of θ_{JC} is to 1.) provide a standardized metric to compare thermal performance of different package options and configurations, and 2.) provide a numerical value to predict package level thermal performance and junction temperature. One of the shortcomings of θ_{JC} regarding the second statement, predicting package performance, is that it only applies to a specific set of boundary conditions [6]; a measured θ_{JC} value can change depending on the TIM II and external cooling solution [7]. Secondly, it does not capture the relationship between heat spreading within the package and the external cooling solution (TIM II and heat sink). Since the primary function of a vapor chamber is to enhance the heat spreading compared to pure copper, θ_{JC} is not an ideal metric. Instead, for this study it was decided to use junction temperature (T_j) normalized to ambient temperature (T_{amb}). Using T_j-T_{amb} to compare the differences between copper and VC heat spreaders will capture the influence of heat spreading on the TIM II and heat sink. Since thermal resistance is a function of area, a larger area of heat flux over the package due to the increased spreading of the VC effectively enables a lower resistance path through the TIM II and heat sink base. Therefore, it is critical to capture the interaction of the VC heat spreader with the TIM II and heat sink to characterize the benefit of a VC.

The results proved the expected dependence of vapor chamber heat spreading relative to the TIM II and heat sink thermal resistance, Fig. 6. In the highest thermal resistance condition, thermal pad with aluminum heat sink, the VC heat spreader showed a dramatic improvement of 12.5°C reduction in normalized junction temperature relative to a standard copper lid at 120W power. The aluminum heat sink and grease TIM II condition showed a 6.3°C reduction in normalized junction temperature for the VC heat spreader compared to the standard copper heat spreader. The lowest thermal resistance cooling solution, copper heat sink with grease type TIM II, showed a 4.2°C reduction in junction temperature for the VC heat spreader relative to the standard copper heat spreader.

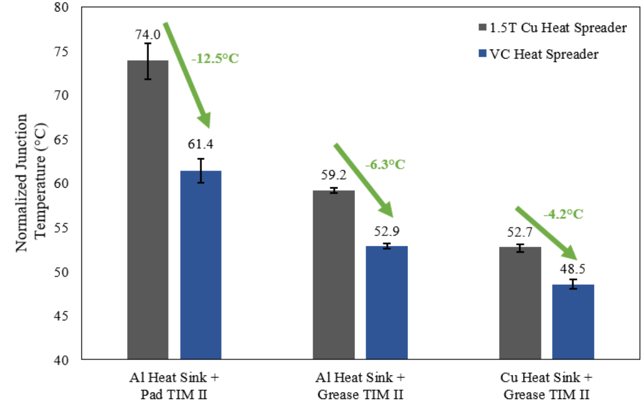

Fig. 6. Thermal measurement data for VC and Cu heat spreaders.

VII. VAPOR CHAMBER CHARACTERIZATION

In addition to measuring the impact of junction temperature and thermal resistance of vapor chamber heat spreaders, it is important to understand effective thermal conductivities they can achieve under the various test conditions in this study. The results demonstrated that the reduction in junction temperature due to the vapor chamber heat spreader was not constant with respect to the different TIM II and heat sink conditions. Therefore, it can be deduced that if all other variables are fixed, the vapor chamber heat spreader must have varying thermal resistance and ultimately thermal conductivity, depending on the external boundary conditions (TIM II and heat sink).

Thermal conductivity or thermal resistance is not a property that can be measured directly - it can only be inferred by making measurements according to Fourier's Law of conduction (2).

$$\dot{Q} = -kA\frac{\Delta T}{L} \quad (2)$$

Where $\dot{Q}$ is the amount of heat transferred per unit time, k is the conductivity of the material in $Wm^{-1}.K^{-1}$, A is the area of the cross-sectional surface, ΔT is the temperature difference between the endpoints, and L is the distance between two ends.

However, this law is only valid when considering uniform 1-dimensional heat conduction. In an FCBGA package, heat flow is highly multidirectional. In a previous work [8], a method was developed for extracting the localized thermal resistance of thermal interface materials in an FCBGA

package using finite element analysis along with empirical measurements. A similar approach was used for this study to extract the effective thermal conductivity of the vapor chamber heat spreaders.

An FEA model was constructed to capture the details of the thermal test setup including test board, package designs, external cooling solution, and environmental conditions. To extract the effective thermal conductivity of the vapor chamber heat spreaders, the experimental measurements of chip temperature and power are input into the simulation. Comparing the standard heat spreader to the VC heat spreader under the same test conditions, the only variable being changed is the heat spreader. It is assumed that the TIM I, TIM II and heat sink resistances are equivalent between tests. In addition, the environmental conditions are controlled and accounted for in the measurements. The vapor chamber heat spreader internal cavity (vapor space and wick structure) was modeled as a single block with an effective thermal conductivity; this value will be the target of the objective function. All other design details of the vapor chamber construction were captured in the model.

An initial value for thermal conductivity is input for the vapor chamber cavity. The simulation is run for both standard and VC heat spreader models, and the maximum junction temperature to ambient temperature delta is calculated and compared. For the next iteration, the vapor chamber cavity thermal conductivity is increased, and the model resolved. This process is repeated for a range of thermal conductivity values spanning typical thermal conductivities of vapor chambers. The objective function (3) is satisfied when the difference in standard heat spreader to VC heat spreader junction temperatures from experimental measurements equals the standard to VC heat spreader junction temperature difference from simulation.

$$\begin{aligned}(T_{j,max} - T_{amb})_{CuHS,EXP} - (T_{j,max} - T_{amb})_{VCHS,EXP} \\ = \\ (T_{j,max} - T_{amb})_{CuHS,SIM} - (T_{j,max} - T_{amb})_{VCHS,SIM}\end{aligned} \qquad (3)$$

Where $T_{j,max}$ is the maximum junction temperature of the thermal chip, T_{amb} is the ambient temperature measured experimentally or input into model.

The subscripts in equation (3) "CuHS,EXP" refer to the measured data on the standard copper heat spreader, "VCHS, EXP" refers to the measured data on the VC heat spreader, and the "SIM" subscript refers to the simulation data of the same terms. Linear interpolation was preformed between simulation data points to calculate the VC effective thermal conductivity at the experimental data intercept. The Al heatsink and grease TIM II case could not be evaluated for effective thermal conductivity due to inadequate sample size.

Using the method defined for extracting the effective thermal conductivity of the vapor chamber cavity, it was found that the test condition with an aluminum heat sink and pad type TIM II resulted in an effective vapor chamber thermal conductivity of 11,750 W/m*K. For the test condition with copper heat sink and grease type TIM II, the resulting effective thermal conductivity of the vapor chamber was 3,495 W/m*K. These results demonstrate the vapor chamber's dependency on temperature gradient and external heat transfer conditions. The aluminum heat sink and pad TIM II have a higher temperature gradient across the base of the heat sink compared to the copper heat sink and grease TIM II. This higher gradient allows the increased efficiency of the vapor chamber to achieve greater effectiveness over a broad range.

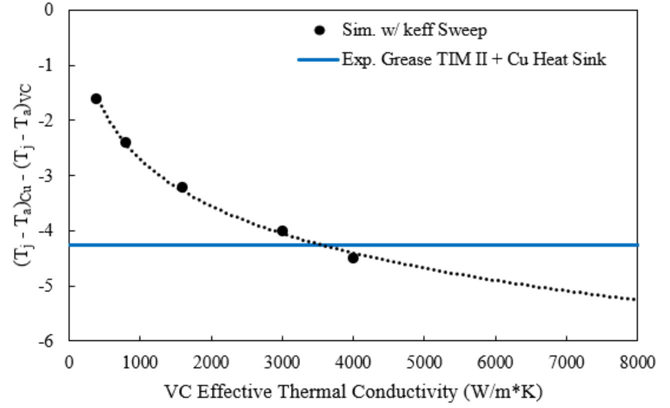

Fig. 7. Simulation data with sweep of VC heat spreader effective thermal conductivity and experimental data point for grease TIM II and copper heat sink DOE condition. Extracted effective thermal conductivity of the vapor chamber was 3,495 W/m*K as seen by the intersection of two curves in this chart.

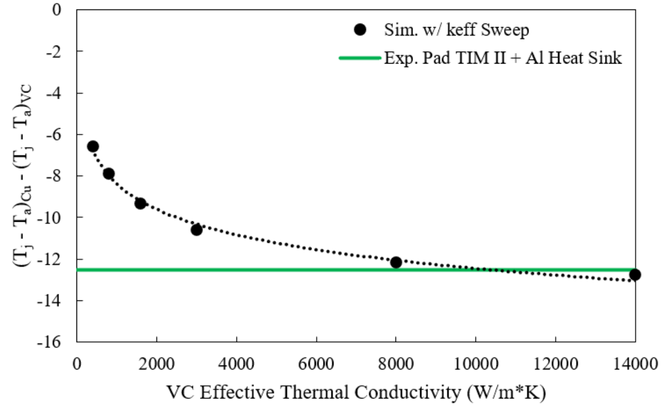

Fig. 8. Simulation data with sweep of VC heat spreader effective thermal conductivity and experimental data point for pad type TIM II and aluminum heat sink DOE condition. Extracted effective thermal conductivity of the vapor chamber was 11,750 W/m*K as seen by the intersection of two curves in this chart.

VIII. Uncertainity Analysis

To determine the validity of using this approach to extract the effective thermal conductivity of the vapor chamber heat spreaders, an uncertainty analysis was conducted. Ultimately, the goal of any measurement will be to minimize the level of uncertainty to the point where the total error has a low sensitivity on the target measurement. The test leg pairs in this study were setup to ensure the only variable changing between legs was the heat spreader type used. In relation to the FEA model for extracting vapor chamber thermal conductivity, the model is attempting to capture a differential value; the junction temperature difference between the lid

types, rather than attempting to predict the absolute value of the junction temperature. With all variables fixed, it could be assumed that the uncertainty between each test was reasonably equivalent. Therefore, if the heat conduction paths are adequately captured in the model, it could be surmised that the junction temperature difference captured between the copper heat spreader and VC heat spreader were reasonably predicted.

IX. Conclusion

This investigation revealed that a FCBGA package integrated vapor chamber heat spreader can offer significant thermal enhancement over a traditional copper heat spreader for certain applications. In determining the applicability of vapor chamber heat spreaders, the package end use system thermal solution needs to be considered. For extremely low thermal resistance heat sinks, such as those implementing vapor chambers, heat pipes and / or liquid cooling, a package level vapor chamber may offer little improvement in thermal performance. However, for higher resistance heat sinks, such as copper or aluminum air cooled, a package level VC heat spreader can provide significant thermal enhancement. The system TIM II should also be considered as a contributing factor. With a high thermal resistance material, a VC heat spreader can spread heat over a larger more uniform area before conducting through the TIM. Whereas a very low resistance material does not have the same influence on heat spreading in the vapor chamber. Lastly, the package design itself determines if a vapor chamber heat spreader can operate efficiently. While the range of effectiveness was not evaluated in this study, it is recommended the package body to die area ratio should be a minimum of 5:1. However, silicon designs with high power density hot spots can still benefit tremendously even in package to die ratio is less than 5:1. This study also proposed an effective method for evaluating the effective thermal conductivity of a vapor chamber heat spreader using a calibrated FEA model. With reasonable uncertainty, the FEA model was able to extract the effective thermal conductivity of the vapor chamber heat spreader for each of the test conditions. Using this model, the test condition with an aluminum heat sink and pad type TIM II resulted in an extracted effective vapor chamber thermal conductivity of 11,750 W/m*K. For the test condition with copper heat sink and grease type TIM II, the extracted effective thermal conductivity of the vapor chamber was 3,495 W/m*K.

© 2023, Amkor Technology, Inc. All rights reserved.

References

[1] C. Nelson, "Thermal Management Implications for Heterogeneous Packaging," 16th Internation Conference and Exhibition on Device Packaging, 2020.

[2] M. Bulut, S. Kandlikar, N. Sozbir, "A Review of Vapor Chambers," in Heat Transfer Engineering, 2018

[3] M. Gibbons, M. Marengo, T. Persoons, "A Review of Heat Pipe Technology for Foldable Electronic Devices," in Applied Thermal Engineering, vol 194, 2021.

[4] R. Mahajan, "Thermal Interface Materials: A Brief Review of Design Characteristics and Materials," Electronics Cooling, February 1st, 2004.

[5] R. Prasher, J. C. Matayabas Jr, "Thermal Contact Resistance of Cured Gel Polymeric Thermal Interface Material," IEEE Transactions on Components and Packaging Technologies, Vol. 27, No. 4, December 2004.

[6] J. Galloway, S. Bhopte, "Characterizing Junction-to-Case Thermal Resistance and Its Impact on End-Use Applications," SEMI-THERM 28th Symposium, IEEE, 2012.

[7] J. Galloway, E. De Los Heros, "Developing a ThetaJC Standard for Electronic Packages," SEMI-THERM 34th Symposium, IEEE, 2018.

[8] C. Nelson, J. Galloway, P. Fosnot, "Extracting TIM Properties with Localized Transient Pulses," SEMI-THERM 30th Symposium, pp. 72 - 80. IEEE, 2014.